Applied Surface Science 605 (2022) 154820

Contents lists available at ScienceDirect

Applied Surface Science

journal homepage: www.elsevier.com/locate/apsusc

Full Length Article

Eco-friendly sonochemical reduction of graphene oxide in water using TiO_2 photocatalyst activated by sonoluminescence

A. Young Lee [a,1], Seon Ae Hwangbo [a,1], Mun Seok Jeong [b,*], Tae Geol Lee [a,*]

[a] Nanosafety Team, Safety Measurement Institute, Korea Research Institute of Standards and Science, Daejeon 34113, Republic of Korea
[b] Department of Physics and Department of Energy Engineering, Hanyang University, Seoul 04763, Republic of Korea

ARTICLE INFO

Keywords:
Reduced graphene oxide (rGO)
Sonoluminescence
TiO_2 nanoparticles
Photocatalytic effect
Focused ultrasound

ABSTRACT

Reduced graphene oxide (rGO) is a representative commercialized graphene-related material that can be mass-produced. However, the conventional thermal and chemical reduction methods require high temperatures and toxic reducing agents and consume energy and cause environmental pollution. Therefore, alternative eco-friendly methods that are less energy-intensive are required for their mass production. Herein, we propose a facile and eco-friendly reduction method that enables the mass production of rGO. Specifically, a custom-built focused ultrasound circulation system was used to reduce graphene oxide in a suspension without using toxic reagents. The sonicated rGO was reduced to a significant extent, and its carbon-to-oxygen atomic ratio (87.79%) and electrical conductance (9.15 μS) were comparable to those of commercially available rGO. Raman spectroscopic analysis revealed that sonicated rGO gave a lower D-to-G band intensity ratio than commercial rGO reduced by heat treatment. This method can contribute to the active utilization of rGO in next-generation industrial products with lower environmental and energy impacts.

1. Introduction

Graphene is a carbon material that comprises single atomic layers of graphite with a honeycomb carbon structure. Graphene offers a large specific surface area [1], exceptional electrical and thermal transport properties [2,3], and high mechanical strength [4], and therefore has drawn considerable attention for various applications, such as in electronic devices, biosensors, flexible devices, and electrocatalysts [5–12]. Novoselov et al. developed a mechanical exfoliation method for obtaining defect-free monolayer graphene [13], and the advent of this effective peel-off method has led to extensive studies on the intriguing intrinsic properties of graphene [14,15]. However, the mass-production of graphene sheets using this approach is challenging, which has restricted the industrial use of graphene. Many groups have attempted to produce graphene on a large scale via chemical vapor deposition and epitaxial growth [16–18]. However, these bottom-up methods rely on high temperatures and ultra-high vacuum conditions, which further hinders the commercial application of graphene. The production of reduced graphene oxide (rGO) has been proposed for the commercialization of graphene. The current methods for manufacturing rGO involve the intentional oxidization of graphite to obtain carbon layers with oxygen-containing functional groups on the basal plane [19,20]; then, the hydrophilic graphite oxide is exfoliated to graphene oxide (GO) in water under sonication. The oxygen groups are subsequently removed from GO to obtain conductive GO because the absence of percolating pathways in sp^2 carbon clusters results in insulating properties [21].

The degree of reduction of exfoliated GO determines its physicochemical properties [22,23], and thus many studies have focused on the development of effective reduction methods [24,25] and have evaluated the degree of reduction [26,27]. Thermal reduction, one of the most commonly used methods for GO reduction, consumes considerable energy because it requires temperatures above 1000 °C and can cause thermal damage to rGO and mass loss [28–30]. Another popular approach is to employ chemical reducing agents such as hydrazine hydrate [31], dimethylhydrazine [32], and sodium borohydride,[24] which are toxic and harmful to workers and the environment. In recent years, the demand for reduction methods that are safe, controllable, and

Abbreviations: GO, graphene oxide; rGO, reduced graphene oxide; FESEM, field-emission scanning electron microscopy; TEM, transmission electron microscopy; XPS, X-ray photoelectron spectroscopy; CPS, centrifugal particle sizer; c-AFM, conductive atomic force microscopy.

* Corresponding authors.
E-mail addresses: mjeong@hanyang.ac.kr (M. Seok Jeong), tglee@kriss.re.kr (T. Geol Lee).

[1] These authors contributed equally to the work.

https://doi.org/10.1016/j.apsusc.2022.154820
Received 16 June 2022; Received in revised form 24 August 2022; Accepted 4 September 2022
Available online 7 September 2022

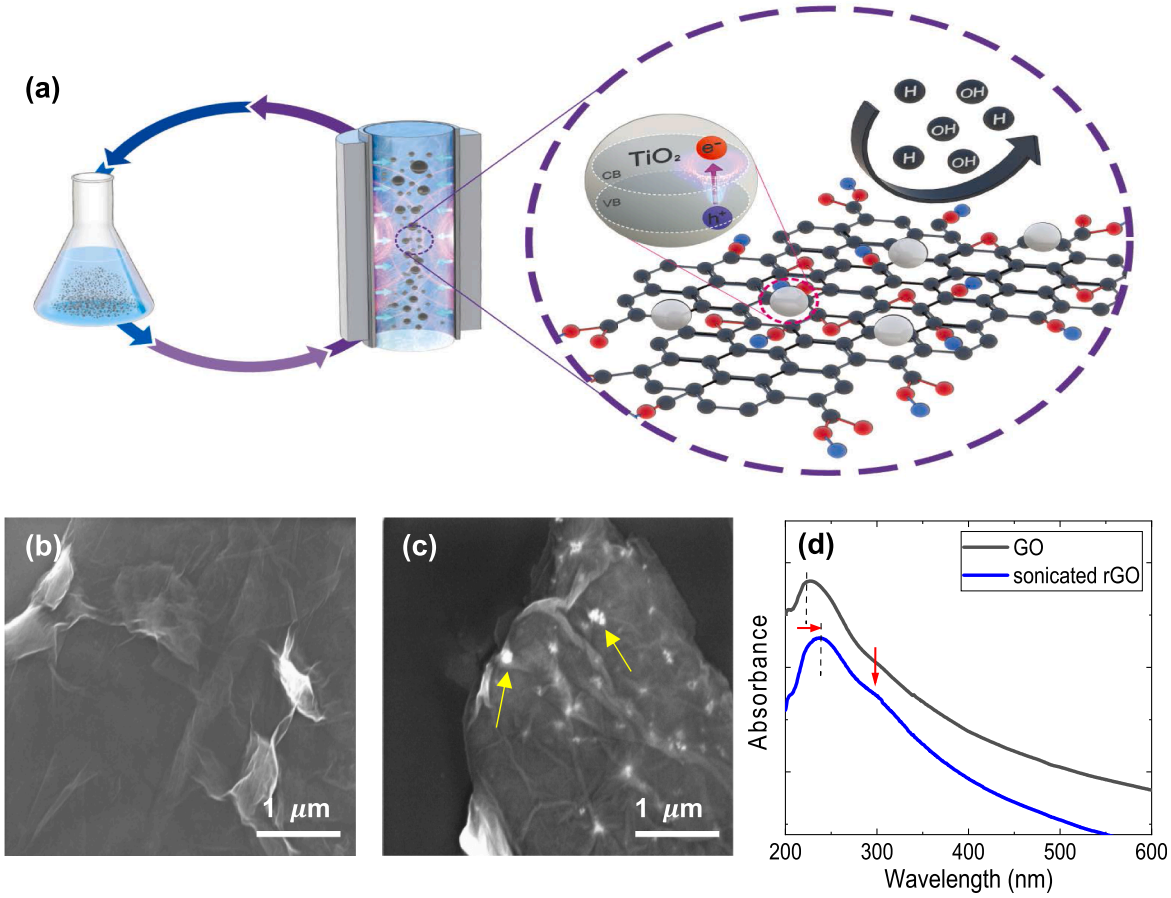

Fig. 1. (a) Schematic illustration of GO reduction based on the synergistic effect between photocatalytic TiO_2 nanoparticles and free radicals generated via sonication in the focused ultrasound dispersion system. SEM images of (b) commercial GO sample and (c) sonicated rGO with aggregated TiO_2 nanoparticles (yellow arrows). Scale bar represents 1 μm. (d) UV–vis absorption spectra of GO (gray) and sonicated rGO (blue).

environmentally friendly for the economical production of high-quality rGO has increased. Photocatalytically active semiconductor-based materials are promising candidates for the eco-friendly production of rGO, because high-volume production capacity in the aqueous state can be realized without the use of large amounts of energy or chemical reactions with toxic reagents. TiO_2 nanoparticles are one of the most widely used photocatalytic semiconductors, as they are relatively inexpensive, innocuous, and chemically inert. Furthermore, TiO_2-rGO nanocomposites have excellent properties, such as improved photoelectrochemical activity [33] and thermal conductivity compared to those of TiO_2 [34].

Focused ultrasound circulation is an eco-friendly reduction method that relies on ultrasonic effects to eliminate oxygen. This approach can also be applied to the mass-production of GO via the exfoliation of GO in the solution state [35]. Specifically, ultrasonic waves dissociate water into OH· and H· radicals under the high pressure and high temperature generated as water droplets collapse. These free radicals interact with and remove the oxygen functional groups on the GO carbon planes. According to a previous report, a sonic bath and sonic probe can be used to achieve reduction ratios of 68.9% and 70.8%, respectively [36]. However, conventional bath systems and horn-type sonic systems only expand and contract water molecules near the ultrasound source, thereby leading to partial reduction of the substrate. Instead, the circulation of the liquid medium in a focused ultrasound system can facilitate energy transfer throughout the liquid to achieve uniform exfoliation and reduction. Considering the merits of photocatalytic reduction and focused ultrasound, a combined approach based on free radicals and the photocatalytic effect of TiO_2 nanoparticles can be promising for the simple and eco-friendly production of high-quality rGO on an industrial scale.

In this study, we developed a simple and eco-friendly reduction approach for the mass-production of high-quality rGO based on a synergistic process involving free radicals produced using ultrasound and photocatalytic TiO_2 nanoparticles. A custom-built focused ultrasound circulation system was used, which generated strong acoustic fields for producing intense ultraviolet light via sonoluminescence [37], to activate the TiO_2 photocatalyst without using a pulsed laser [38,39]. A high degree of GO reduction was achieved, and the resulting rGO had a carbon-to-oxygen (C/O) atomic ratio of 7.83 (i.e., relative content of carbon to oxygen of 87.79%). In addition, the rGO contained few defects and exhibited an excellent electrical conductance of 9.15 μs.

2. Experimental

2.1. Preparation and characterization of TiO_2 nanoparticles

A TiO_2 nanoparticle suspension was purchased from Sigma-Aldrich (P25, Evonik). The size and shape of the nanoparticles were determined by transmission electron microscopy (TEM; JEM-ARM200F, JEOL) at an accelerating voltage of 150 kV. TEM samples were prepared by diluting the suspension with deionized water, and then drop-casting it onto a TEM grid covered with a carbon film. The particle size was measured using a centrifugal particle sizer (CPS) disc centrifuge (CPS Disc Centrifuge UHR, CPS Instruments Europe). The ultraviolet–visible (UV–vis) absorption spectrum of the TiO_2 nanoparticles was obtained in the spectral range of 200 nm to 800 nm to confirm that

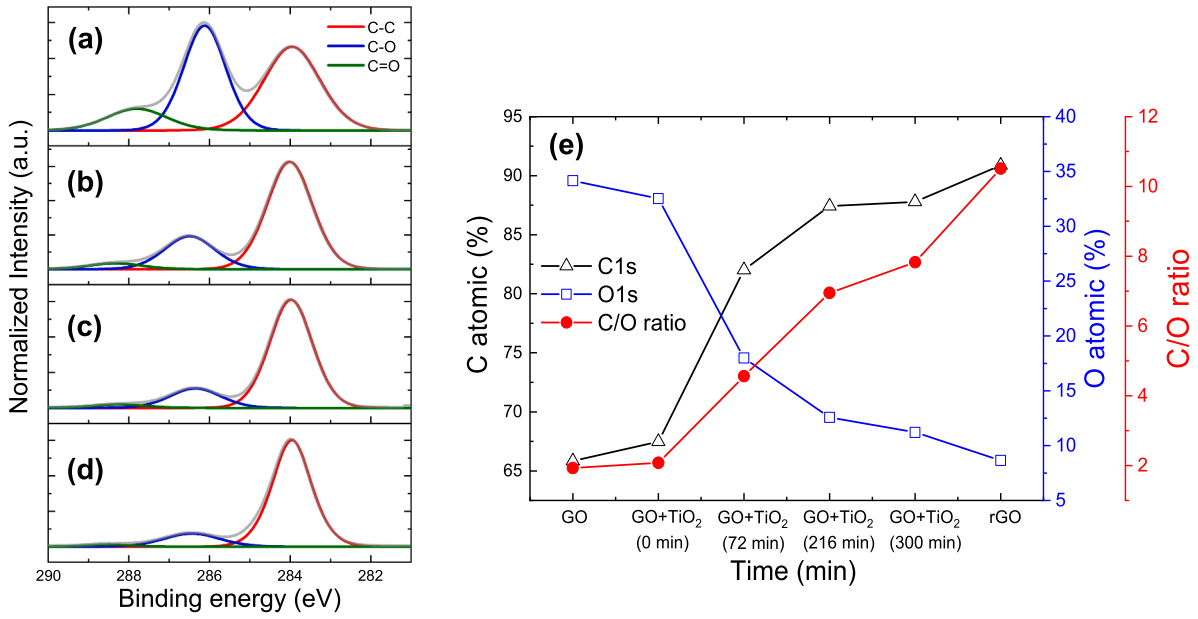

Fig. 2. C1s XPS profiles of (a) GO combined with TiO_2 nanoparticles before sonication, and after sonication for (b) 72, (c) 216, and (d) 300 min. (e) Change in the atomic ratios of carbon (black triangles) and oxygen (blue squares), and the C/O atomic ratio (red circles) during exposure to sonoluminescence.

the UV light-induced excitation of electrons from the valence band to the conduction band of the semiconductor (UV-1800, Shimadzu Scientific Instruments Inc.) [40].

2.2. Preparation of sonicated rGO

GO (GO-V50) and rGO (rGO-V50) were purchased from Standard Graphene Inc. Sonicated rGO was prepared by adding 30 mL of a TiO_2 suspension (0.01 wt%) to 100 mL (0.2 wt%) of the GO suspension under 400 kHz, 150 W conditions of a focused ultrasound system[41].

2.3. Characterization of GO, rGO, and sonicated rGO

The surface morphologies of GO, rGO, and sonicated rGO were compared by field-emission scanning electron microscopy (FESEM, S-4800 Hitachi, Japan). The elemental compositions of GO, rGO, and sonicated rGO were analyzed by X-ray photoelectron spectroscopy (XPS) using Cu-Kα radiation at an acceleration voltage of 5 keV (K-alpha + MXP10, Thermo Fisher Scientific). The C/O atomic ratio was determined based on XPS measurements; the oxygen signal due to SiO_2 on the silicon substrate surface was excluded from the measurements by coating the silicon substrate with an Au film (thickness = 100 nm).

Raman scattering was performed using a laser with a wavelength of 532 nm at a power of 0.1 mW. A 100 × objective lens (0.9NA) and a grating with 1800 grooves/mm for an exposure time of 120 s (Alpha300, WItec) were used in the analysis. Raman spectra were acquired in the spectral range of 1000 to 1900 cm^{-1}, and all spectra were fitted with combinations of Lorentzian curves with R-squared values higher than 0.9. UV–vis absorption spectra were acquired in the spectral range from 200 to 600 nm.

The electrical properties were evaluated based on electrical conductance measurements using conductive atomic force microscopy (c-AFM; XE7, Park Systems Inc.) (**Figure S1**). Indium tin oxide glass was introduced as a conductive substrate to carry the current between the metal-coated section of the cantilever and the sample holder. The current distribution was measured at a sample bias of 10 V using an internal current amplifier at a gain value of 109 V/A, where the recommended current range is 10 pA to 10nA. The heterogeneity of the local electrical properties was visualized within a scan area of 10 μm × 10 μm (256 pixels × 256 lines) at a point distance of 39 nm. All conductance values were based on an average of nine measurements performed at different arbitrary positions.

3. Results and discussion

3.1. Proposed GO reduction method

The proposed reduction process of GO relies on the photocatalytic effect of TiO_2 nanoparticles activated by sonoluminescence on the carbon plane and the removal of oxygen functional groups by the free radicals (e.g., H· and OH·) generated via the dissociation of water under ultrasonication (Fig. 1**(a)**) [41]. The free radicals were produced due to the high temperature and high pressure generated by the friction of collapsing cavitation bubbles. The free radicals attacked the oxygen functional groups to produce CO_2, resulting in the reduction of GO [36].

3.2. Morphological analysis

The TiO_2 nanoparticles had a particle size of ~60 nm (mode value) **(Figure S2)**, and the UV–vis absorption spectrum indicated that UV light excited an electron from the valence band to the conduction band of the semiconductor [40].

The FE-SEM images of commercial GO and sonicated rGO nanoparticles were compared (Fig. 1**(b) and (c)**). The sonication method successfully yielded a graphene/ TiO_2 nanocomposite, and fewer wrinkles were observed in the carbon layer. This indicated that the heat generated by sonication had a negligible effect on the GO/rGO structure. Comparison of the SEM images of commercial rGO, which was prepared by the heat-treatment method, with the sonicated rGO obtained by the proposed method (**Figure S3**) confirms a less wrinkled structure for rGO (**Figure S3(b, c)**). That is, high temperature used in the thermal reduction process causes thermal shock, which disrupts the sp^2 carbon hybridization [42]. The aggregation of TiO_2 nanoparticles on the carbon layer of the sonicated rGO was observed, but this aggregated state did not significantly affect the photocatalytic activity [43].

The UV–vis absorption spectra of pristine GO and sonicated rGO exhibited distinctive differences in peak position (Fig. 1**(d)**). The spectrum of GO included a peak at 230 nm, which was attributed to π–π* transition of the C=C bond. This peak was red-shifted during reduction due to the recovery of the conjugated bonds in the graphene sheets

Table 1
Atomic percentages of carbon and oxygen, and the C/O ratio of GO before and after sonication with TiO_2 nanoparticles.

Sample	%C	%O	C/O ratio
Pristine GO	65.84	34.16	1.93
GO + TiO_2 (0 min)	67.48	32.52	2.08
GO + TiO_2 (72 min)	82.02	17.98	4.56
GO + TiO_2 (216 min)	87.42	12.58	6.95
GO + TiO_2 (300 min)	87.79	11.21	7.83
Commercial rGO	90.87	8.65	10.51
PS120 [36]	70.8	29.2	2.4

under sonication [44]. Further, the intensity of the broad peak at 300 nm, attributed to the carbonyl group (C=O), decreased after sonication as the oxygen functional groups were removed [45].

3.3. XPS analysis

The C1s XPS profiles of the sonicated rGO exhibited a peak corresponding to C–C bonds at ~284 eV, a peak of C–O bonds such as epoxides at ~286 eV, and a peak of carbonyl groups (C=O) at ~288 eV (Fig. 2**(a), (b), (c), and (d)**) [46,47]. Considering the correlation between the exposure time of sonoluminescence and the C/O ratio determined by the XPS peak analysis (Fig. 2 **(e)**), the oxygen-containing functional groups were gradually removed as the duration of exposure increased. As sonoluminescence determined the quantity of oxygen-containing groups, the photocatalytic performance of TiO_2 was a key factor in controlling the degree of reduction of GO. In the absence of sonoluminescence, the GO + TiO_2 sample (0 min) did not undergo reduction, and thus the C/O ratio was similar to that of pristine GO. This was further confirmed by the absorption peak positions in the UV–vis spectra of pristine GO, GO + TiO_2 (not sonicated), and sonicated GO + TiO_2 (72 min) (**Figure S4**).

The C/O atomic ratio increased during sonication (Table 1). In the case of GO + TiO_2 (300 min), which was subjected to the longest sonication process among the sonicated rGO samples in this study, the reduction degree approached 87.79% with a C/O ratio of 7.83, which is comparable to that of commercial rGO.

Table 1 also shows the data obtained for PS120 (reduction of graphene oxide by performing probe sonication) from a study conducted by Le et al. [36] for comparison. Compared to the previous results of probe sonic, the GO reduction using the focused ultrasound circulation system presented here results in a three-fold increase in the C/O ratio. These findings demonstrate that a high degree of reduction can be achieved via the photocatalytic effect of TiO_2 and the ultrasonic effect at high power.

3.4. Raman spectroscopy

The fitted Raman spectra of pristine GO, sonicated rGO, and thermally reduced rGO in the spectral range of 1000 to 1900 cm^{-1} were compared (Fig. 3**(a), (b), and (c)**). Five Lorentzian profiles were used to fit the Raman peaks and obtain the intensities and wavenumbers of the components, viz., the D, G, D', D'', and D* bands. A G band located at

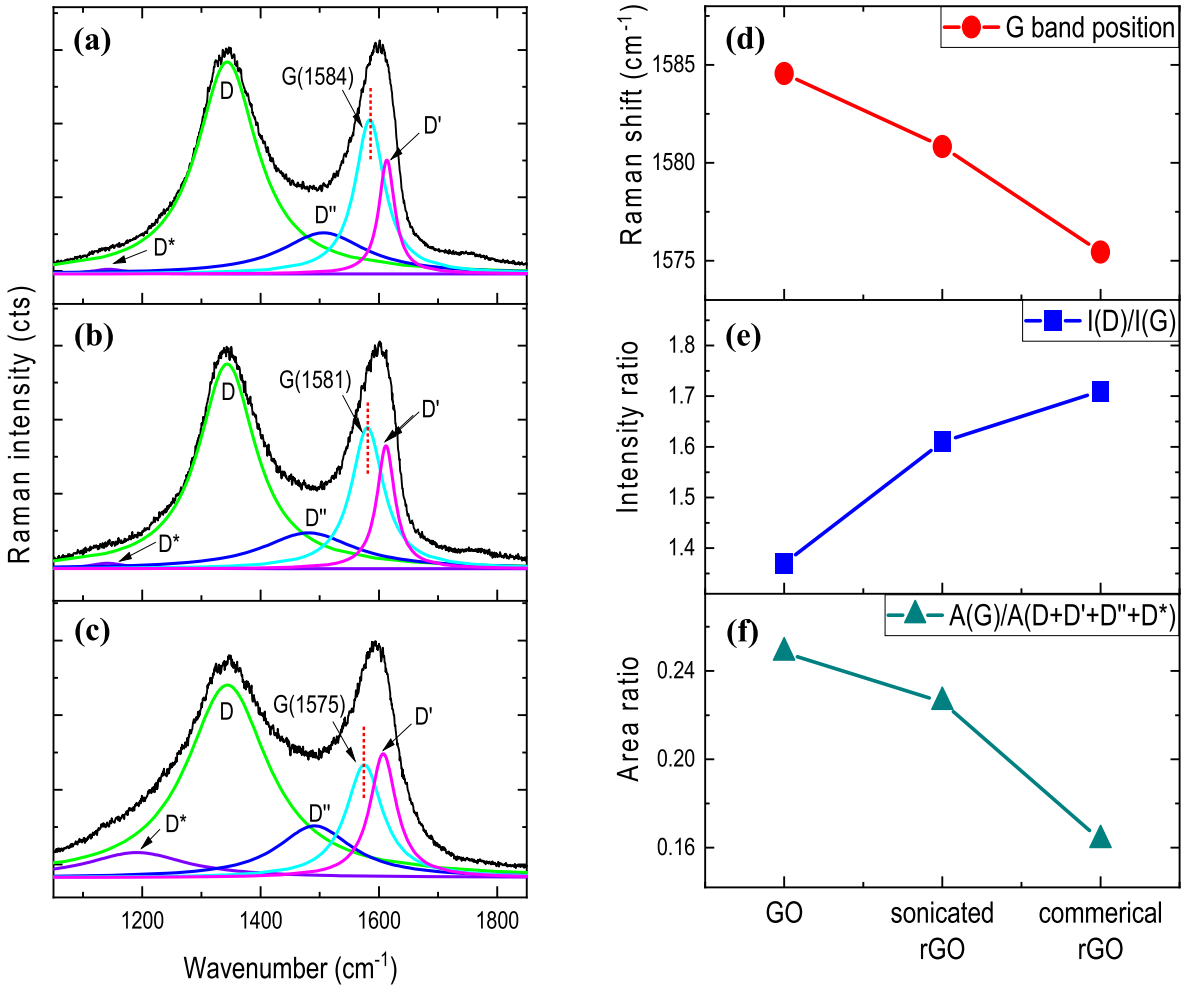

Fig. 3. Fitted Raman spectra of (a) pristine GO, (b) sonicated rGO (300 min), and (c) commercial rGO, and the corresponding (d) Raman shift of the G band, (e) I(D)/I(G) ratio, and (f) Raman area ratio of the G band and other bands (D, D', D'', and D* bands).

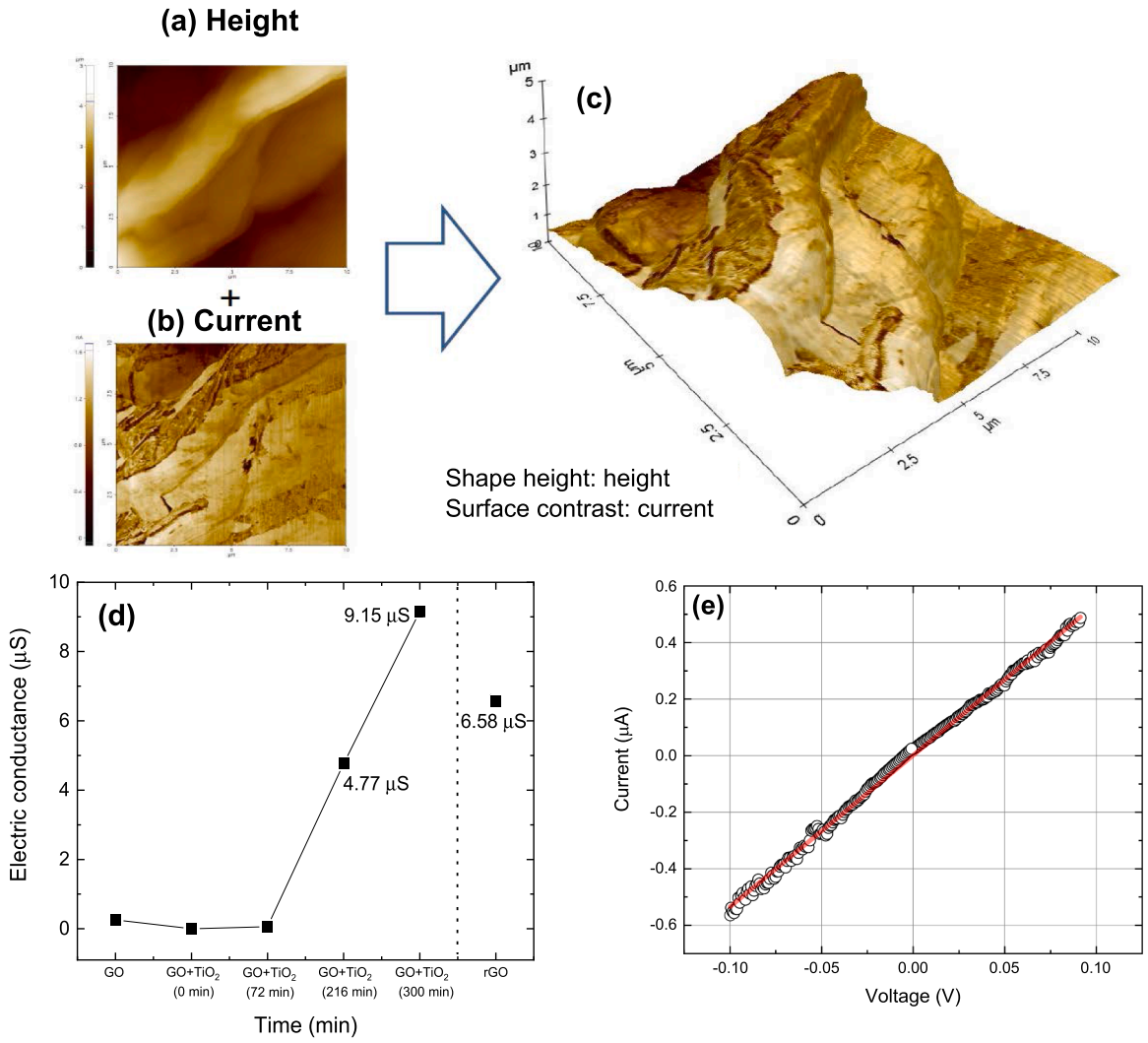

Fig. 4. c-AFM measurements of sonicated rGO given as (a) height distribution, (b) current distribution, and (c) volumetric representation of current distribution according to height. (d) Electric conductances of pristine GO, sonicated GO with TiO_2 according to the sonication time, and commercial rGO (thermally reduced), (e) I–V curve of sonicated rGO (300 min).

~1583 cm^{-1} was observed for all types of carbon materials owing to the E_{2g}-symmetrical vibration mode in the sp^2 phase of carbon [48]. The red-shift of the G band for the sonicated rGO relative to that of pristine GO can be attributed to its higher degree of reduction (Fig. 3**(d)**) [23]. XPS analysis (Fig. 2) confirmed the relatively lower degree of reduction of the sonicated rGO compared to that of commercial rGO, and thus the sonicated rGO exhibited a smaller Raman shift of the G band.

Another intense peak in the Rama spectra is the D band related to the disordered structure of the carbon plane. Based on the origins of the D band and G band, the intensity ratio of the D to G band is inversely related to the crystallite size of carbon materials[49], which is one of the factors that determine the electrical property. The I(D)/I(G) of the sonicated rGO was lower than that of commercial rGO, indicating that the proposed ultrasonic treatment method facilitated the synthesis of higher-quality rGO compared to conventional reduction processing (Fig. 3**(e)**). This comparative spectral analysis provided an indication of the quality of the rGO and suggested that the sonicated rGO could afford better electric conductance at a lower degree of reduction.

The D* band is related to the sp^3-rich phase [50], while the D'' band (~1500 cm^{-1}) is attributed to the amorphous carbon fraction and the D' band (~1620 cm^{-1}) is attributed to intra-valley resonance with G band splitting due to impurities [51]. The sonicated GO was quantitatively evaluated by comparing the sum of phonon vibration scattering due to the sp^3 phase, impurities, and defects other than the G band (i.e., the vibration of sp^2 carbons) (Fig. 3**(f)**). The comparative analysis of the area ratios of the G band and the other bands (D band, D* band, D' band, and D" band) revealed that the sonicated rGO had fewer defects than commercialized rGO prepared via conventional thermal treatment.

3.5. Electrical properties

All the samples evaluated in this study were wrinkled, even within a single flake, and different areas had different thicknesses. Therefore, their electrical characteristics varied depending on the location. Therefore, the electrical evaluation of sonicated rGO was conducted by determining the current distribution according to sample height. The height distribution was analyzed (Fig. 4 **(a)**) by AFM topographic analysis, and the current characteristics were imaged within the same area via c-AFM (Fig. 4**(b)**). The height distribution and current characteristic data obtained using c-AFM were combined to produce a mapping image of the electrical features according to the height of the sonicated rGO (Fig. 4**(c)**).

To compare the electrical properties of GO, sonicated rGO, and commercial rGO (thermally reduced), the averaged electric conductance values were obtained based on measurements at nine random positions (Fig. 4**(d)**). Sonicated rGO exhibited a gradual increase in conductance

from pico siemens (pS) to micro siemens (μS) with increasing sonication time. A comparison of the conductance of the sonicated rGO (300 min) and commercial rGO samples revealed that the sonicated rGO affords higher conductance (9.15 μS) than commercial rGO (6.58 μS), despite its lower C/O ratio. This indicated that the electrical conductance is related to both the degree of reduction and the quality of the carbon structure [24].

The current–voltage (I–V) curves of sonicated rGO (300 min) exhibited strong linearity between the current and voltage, indicative of Ohmic characteristics (Fig. 4**(e)**). The average current and conductance values are given in **Table S1**. The I–V curves obtained before and after scraping the surface of the sonicated rGO are shown in **Figure S5**, because the electrical measurements are sensitive to surface contaminants. The effect of contaminants on the inherent properties of the sample was minimized by conducting surface cleaning via scraping with a diamond-coated cantilever (hardness = ~8700 nM).

4. Conclusions

The high-power sonication of a GO suspension in water using a focused ultrasound system effectively induced the sonochemical reduction of GO by free radicals and photocatalytic reduction of GO under the activation of TiO_2 nanoparticles by sonoluminescence, resulting in high-quality rGO. A less wrinkled structure of the sonicated rGO was observed in SEM images, which revealed that the thermal energy from sonication is not the primary cause of the removal of the oxygen functional groups. The C/O ratio determined from XPS profiles increased with increasing sonication time, indicating that the photocatalytic effect of TiO_2 plays a primary role in determining the degree of reduction in the absence of a pulsed laser. The changes in the Raman shifts and the ratio of the D and G band intensities suggested that the sonicated rGO has a lower defect density, resulting in superior conductance to that of the commercial rGO. The synergistic effect of the TiO_2 photocatalyst under sonoluminescence provided an efficient and eco-friendly preparation method for high-quality rGO, which can be applied in various industries, such as in electronic and environmental devices.

CRediT authorship contribution statement

A. Young Lee: Conceptualization, Writing – original draft, Data curation, Formal analysis. **Seon Ae Hwangbo:** Conceptualization, Methodology, Writing – original draft, Visualization, Supervision. **Mun Seok Jeong:** Writing – review & editing, Project administration. **Tae Geol Lee:** Writing – review & editing, Funding acquisition.

Declaration of Competing Interest

The authors declare that they have no known competing financial interests or personal relationships that could have appeared to influence the work reported in this paper.

Acknowledgements

This work was supported by the Nano Material Technology Development Program (No. 2016M3A7B6908929) of the National Research Foundation (NRF) funded by the Ministry of Science and ICT, the Development of Measurement Standards and Technology for Biomaterials and Medical Convergence funded by the Korea Research Institute of Standards and Science (KRISS – 2022 – GP2020-0006).

Appendix A. Supplementary data

Supplementary data to this article can be found online at https://doi.org/10.1016/j.apsusc.2022.154820.

References

[1] F. Bonaccorso, L. Colombo, G. Yu, M. Stoller, V. Tozzini, A.C. Ferrari, R.S. Ruoff, V. Pellegrini, Graphene, related two-dimensional crystals, and hybrid systems for energy conversion and storage, Science 347 (2015) 1246501, https://doi.org/10.1126/science.1246501.
[2] A.A. Balandin, S. Ghosh, W. Bao, I. Calizo, D. Teweldebrhan, F. Miao, C.N. Lau, Superior thermal conductivity of single-layer graphene, Nano Lett. 8 (2008) 902–907, https://doi.org/10.1021/nl0731872.
[3] K.I. Bolotin, K.J. Sikes, J. Hone, H.L. Stormer, P. Kim, Temperature-dependent transport in suspended graphene, Phys. Rev. Lett. 101 (2008), 096802, https://doi.org/10.1103/PhysRevLett.101.096802.
[4] C. Lee, X. Wei, J.W. Kysar, J. Hone, Measurement of the elastic properties and intrinsic strength of monolayer graphene, Science 321 (2008) 385–388, https://doi.org/10.1126/science.1157996.
[5] Y. Qin, H.H. Wu, L.A. Zhang, X. Zhou, Y. Bu, W. Zhang, F. Chu, Y. Li, Y. Kong, Q. Zhang, D. Ding, Y. Tao, Y. Li, M. Liu, X.C. Zeng, Aluminum and nitrogen codoped graphene: Highly active and durable electrocatalyst for oxygen reduction reaction, ACS Catal. 9 (2019) 610–619, https://doi.org/10.1021/acscatal.8b04117.
[6] C. Biswas, Y.H. Lee, Graphene versus carbon nanotubes in electronic devices, Adv. Funct. Mater. 21 (2011) 3806–3826, https://doi.org/10.1002/adfm.201101241.
[7] S. Priyadarsini, S. Mohanty, S. Mukherjee, S. Basu, M. Mishra, Graphene and graphene oxide as nanomaterials for medicine and biology application, J. Nanostructure Chem. 8 (2018) 123–137, https://doi.org/10.1007/s40097-018-0265-6.
[8] J. Liu, Q. Ma, Z. Huang, G. Liu, H. Zhang, Recent progress in graphene-based noble-metal nanocomposites for electrocatalytic applications, Adv. Mater. 31 (2019) 1800696, https://doi.org/10.1002/adma.201800696.
[9] T. Yoon, J.H. Kim, J.H. Choi, D.Y. Jung, I.J. Park, S.Y. Choi, N.S. Cho, J.I. Lee, Y. D. Kwon, S. Cho, T.S. Kim, Healing graphene defects using selective electrochemical deposition: Toward flexible and stretchable devices, ACS Nano 10 (2016) 1539–1545, https://doi.org/10.1021/acsnano.5b07098.
[10] X. Liu, X. Luo, H. Nan, H. Guo, P. Wang, L. Zhang, M. Zhou, Z. Yang, Y. Shi, W. Hu, Z. Ni, T. Qiu, Z. Yu, J. Bin Xu, X. Wang, Epitaxial ultrathin organic crystals on graphene for high-efficiency phototransistors, Adv. Mater. 28 (2016) 5200–5205, https://doi.org/10.1002/adma.201600400.
[11] C.S. Boland, U. Khan, G. Ryan, S. Barwich, R. Charifou, A. Harvey, C. Backes, Z. Li, M.S. Ferreira, M.E. Möbius, R.J. Young, J.N. Coleman, Sensitive electromechanical sensors using viscoelastic graphene-polymer nanocomposites, Science 354 (2016) 1257–1260, https://doi.org/10.1126/science.aag2879.
[12] K.D.G.I. Jayawardena, R. Rhodes, K.K. Gandhi, M.R.R. Prabhath, G.D.M.R. Dabera, M.J. Beliatis, L.J. Rozanski, S.J. Henley, S.R.P. Silva, Solution processed reduced graphene oxide/metal oxide hybrid electron transport layers for highly efficient polymer solar cells, J. Mater. Chem. A 1 (2013) 9922–9927, https://doi.org/10.1039/c3ta11822c.
[13] K.S. Novoselov, A.K. Geim, S.V. Morozov, D. Jiang, Y. Zhang, S.V. Dubonos, I. V. Grigorieva, A.A. Firsov, Electric field in atomically thin carbon films, Science 306 (2004) 666–669, https://doi.org/10.1126/science.1102896.
[14] Y.J. Jeong, J. Jang, S. Nam, K. Kim, L.H. Kim, S. Park, T.K. An, C.E. Park, High-performance organic complementary inverters using monolayer graphene electrodes, ACS Appl. Mater. Interfaces 6 (2014) 6816–6824, https://doi.org/10.1021/am500618g.
[15] P. Gowda, D.R. Mohapatra, A. Misra, Enhanced photoresponse in monolayer hydrogenated graphene photodetector, ACS Appl. Mater. Interfaces 6 (2014) 16763–16768, https://doi.org/10.1021/am503892m.
[16] A. Reina, X. Jia, J. Ho, D. Nezich, H. Son, V. Bulovic, M.S. Dresselhaus, K. Jing, Large area, few-layer graphene films on arbitrary substrates by chemical vapor deposition, Nano Lett. 9 (2009) 30–35, https://doi.org/10.1021/nl801827v.
[17] A. Khan, S.M. Islam, S. Ahmed, R.R. Kumar, M.R. Habib, K. Huang, M. Hu, X. Yu, D. Yang, Direct CVD growth of graphene on technologically important dielectric and semiconducting substrates, Adv. Sci. 5 (2018) 1800050, https://doi.org/10.1002/advs.201800050.
[18] J. Park, W.C. Mitchel, L. Grazulis, H.E. Smith, K.G. Eyink, J.J. Boeckl, D.H. Tomich, S.D. Pacley, J.E. Hoelscher, Epitaxial graphene growth by carbon molecular beam epitaxy (CMBE), Adv. Mater. 22 (2010) 4140–4145, https://doi.org/10.1002/adma.201000756.
[19] W.S. Hummers, R.E. Offeman, Preparation of graphitic oxide, J. Am. Chem. Soc. 80 (6) (1958).
[20] R.K. Singh, R. Kumar, D.P. Singh, Graphene oxide: Strategies for synthesis, reduction and frontier applications, RSC Adv. 6 (2016) 64993–65011, https://doi.org/10.1039/c6ra07626b.
[21] G. Eda, M. Chhowalla, Chemically derived graphene oxide: Towards large-area thin-film electronics and optoelectronics, Adv. Mater. 22 (2010) 2392–2415, https://doi.org/10.1002/adma.200903689.
[22] C. Punckt, F. Muckel, S. Wolff, I.A. Aksay, C.A. Chavarin, G. Bacher, W. Mertin, The effect of degree of reduction on the electrical properties of functionalized graphene sheets, Appl. Phys. Lett. 102 (2013) 1339, https://doi.org/10.1063/1.4775582.
[23] K. Krishnamoorthy, M. Veerapandian, K. Yun, S.J. Kim, The chemical and structural analysis of graphene oxide with different degrees of oxidation, Carbon 53 (2013) 38–49, https://doi.org/10.1016/j.carbon.2012.10.013.
[24] H.J. Shin, K.K. Kim, A. Benayad, S.M. Yoon, H.K. Park, I.S. Jung, M.H. Jin, H. K. Jeong, J.M. Kim, J.Y. Choi, Y.H. Lee, Efficient reduction of graphite oxide by sodium borohydride and its effect on electrical conductance, Adv. Funct. Mater. 19 (2009) 1987–1992, https://doi.org/10.1002/adfm.200900167.

[25] Y. Zhu, S. Murali, M.D. Stoller, A. Velamakanni, R.D. Piner, R.S. Ruoff, Microwave assisted exfoliation and reduction of graphite oxide for ultracapacitors, Carbon 48 (2010) 2118–2122, https://doi.org/10.1016/j.carbon.2010.02.001.
[26] A.Y. Lee, K. Yang, N. Duc, C. Park, S. Mi, T. Geol, Raman study of D* band in graphene oxide and its correlation with reduction, Appl. Surf. Sci. 536 (2021), 147990, https://doi.org/10.1016/j.apsusc.2020.147990.
[27] C. Cao, J.Y. Howe, D. Perovic, T. Filleter, Y. Sun, In situ TEM tensile testing of carbon-linked graphene oxide nanosheets using a MEMS device, Nanotechnology. 27 (2016) 28LT01, https://doi.org/10.1088/0957-4484/27/28/28LT01.
[28] R. Larciprete, S. Fabris, T. Sun, P. Lacovig, A. Baraldi, S. Lizzit, Dual path mechanism in the thermal reduction of graphene oxide, J. Am. Chem. Soc. 133 (2011) 17315–17321, https://doi.org/10.1021/ja205168x.
[29] C. Botas, P. Álvarez, C. Blanco, R. Santamaría, M. Granda, M.D. Gutiérrez, F. Rodríguez-Reinoso, R. Menéndez, Critical temperatures in the synthesis of graphene-like materials by thermal exfoliation-reduction of graphite oxide, Carbon 52 (2013) 476–485, https://doi.org/10.1016/j.carbon.2012.09.059.
[30] E.M. Deemer, P.K. Paul, F.S. Manciu, C.E. Botez, D.R. Hodges, Z. Landis, T. Akter, E. Castro, R.R. Chianelli, Consequence of oxidation method on graphene oxide produced with different size graphite precursors, Mater. Sci. Eng. B Solid-State Mater. Adv. Technol. 224 (2017) 150–157. 10.1016/j.mseb.2017.07.018.
[31] S. Stankovich, D.A. Dikin, R.D. Piner, K.A. Kohlhaas, A. Kleinhammes, Y. Jia, Y. Wu, S.B.T. Nguyen, R.S. Ruoff, Synthesis of graphene-based nanosheets via chemical reduction of exfoliated graphite oxide, Carbon 45 (2007) 1558–1565, https://doi.org/10.1016/j.carbon.2007.02.034.
[32] S. Stankovich, D.A. Dikin, G.H.B. Dommett, K.M. Kohlhaas, E.J. Zimney, E. A. Stach, R.D. Piner, S.B.T. Nguyen, R.S. Ruoff, Graphene-based composite materials, Nature 442 (2006) 282–286, https://doi.org/10.1038/nature04969.
[33] M. Tayebi, M. Kolaei, A. Tayyebi, Z. Masoumi, Z. Belbasi, B.K. Lee, Reduced graphene oxide (RGO) on TiO_2 for an improved photoelectrochemical (PEC) and photocatalytic activity, Sol. Energy 190 (2019) 185–194, https://doi.org/10.1016/j.solener.2019.08.020.
[34] S. Wang, Y. Li, H. Zhang, Y. Lin, Z. Li, W. Wang, Q. Wu, Y. Qian, H. Hong, C. Zhi, Enhancement of thermal conductivity in water-based nanofluids employing TiO_2/reduced graphene oxide composites, J. Mater. Sci. 51 (2016) 10104–10115, https://doi.org/10.1007/s10853-016-0239-3.
[35] R. Durge, R.V. Kshirsagar, P. Tambe, Effect of sonication energy on the yield of graphene nanosheets by liquid-phase exfoliation of graphite, Procedia Eng. 97 (2014) 1457–1465, https://doi.org/10.1016/j.proeng.2014.12.429.
[36] G.T.T. Le, N. Chanlek, J. Manyam, P. Opaprakasit, N. Grisdanurak, P. Sreearunothai, Insight into the ultrasonication of graphene oxide with strong changes in its properties and performance for adsorption applications, Chem. Eng. J. 373 (2019) 1212–1222, https://doi.org/10.1016/j.cej.2019.05.108.
[37] J.S. Jeon, I.J. Yang, J.H. Na, H.Y. Kwak, Radiation mechanism for a single bubble sonoluminescence, J. Phys. Soc. Japan. 69 (2000) 112–119, https://doi.org/10.1143/JPSJ.69.112.
[38] G. Williams, B. Seger, P.V. Kamat, TiO_2-graphene nanocomposites. UV-assisted photocatalytic reduction of graphene oxide, ACS Nano. 2 (2008) 1487–1491, https://doi.org/10.1021/nn800251f.
[39] H. Ogi, M. Hirao, M. Shimoyama, Activation of TiO_2 photocatalyst by single-bubble sonoluminescence for water treatment, Ultrasonics 40 (2002) 649–650, https://doi.org/10.1016/S0041-624X(02)00191-9.
[40] D.A. Panayotov, S.P. Burrows, J.R. Morris, Infrared spectroscopic studies of conduction band and trapped electrons in UV-photoexcited, H-Atom n-doped, and thermally reduced TiO_2, J. Phys. Chem. C 116 (2012) 4535–4544, https://doi.org/10.1021/jp2053103.
[41] S.A. Hwangbo, M. Kwak, J. Kim, T.G. Lee, Novel surfactant-free water dispersion technique of TiO_2 NPS using focused ultrasound system, Nanomaterials 11 (2021) 427, https://doi.org/10.3390/nano11020427.
[42] M.J. McAllister, J.-L. Li, D.H. Adamson, H.C. Schniepp, A.A. Abdala, J. Liu, M. Herrera-Alonso, D.L. Milius, R. Car, R.K. Prud'homme, I.A. Aksay, Single sheet functionalized graphene by oxidation and thermal expansion of graphite, Chem. Mater. 19 (18) (2007) 4396–4404.
[43] T. Degabriel, E. Colaço, R.F. Domingos, K. El Kirat, D. Brouri, S. Casale, J. Landoulsi, J. Spadavecchia, Factors impacting the aggregation/agglomeration and photocatalytic activity of highly crystalline spheroid- and rod-shaped TiO_2 nanoparticles in aqueous solutions, Phys. Chem. Chem. Phys. 20 (2018) 12898–12907, https://doi.org/10.1039/c7cp08054a.
[44] D. Li, M.B. Müller, S. Gilje, R.B. Kaner, G.G. Wallace, Processable aqueous dispersions of graphene nanosheets, Nat. Nanotechnol. 3 (2008) 101–105, https://doi.org/10.1038/nnano.2007.451.
[45] D.C.D.C. Marcano, D.V.D.V. Kosynkin, J.M.J.M. Berlin, A. Sinitskii, Z. Sun, A. Slesarev, L.B.L.B. Alemany, W. Lu, J.M. Tour, Improved synthesis of graphene oxide, ACS Nano 4 (2010) 4806–4814, https://doi.org/10.1021/nn1006368.
[46] K. Dave, K.H. Park, M. Dhayal, Two-step process for programmable removal of oxygen functionalities of graphene oxide: Functional, structural and electrical characteristics, RSC Adv. 5 (2015) 95657–95665, https://doi.org/10.1039/c5ra18880f.
[47] K. Rytel, M. Widelicka, D. Łukawski, F. Lisiecki, K. Kędzierski, D. Wróbel, Ultrasonication-induced sp^3 hybridization defects in Langmuir-Schaefer layers of turbostratic graphene, Phys. Chem. Chem. Phys. 20 (2018) 12777–12784, https://doi.org/10.1039/c8cp01363b.
[48] Y. Wang, D.C. Alsmeyer, R.L. McCreery, Raman spectroscopy of carbon materials: Structural basis of observed spectra, Chem. Mater. 2 (1990) 557–563, https://doi.org/10.1021/cm00011a018.
[49] F. Tuinstra, J.L. Koenig, Raman spectrum of graphite, J. Chem. Phys. 53 (1970) 1126–1130, https://doi.org/10.1063/1.1674108.
[50] J. Schwan, S. Ulrich, V. Batori, H. Ehrhardt, S.R.P. Silva, Raman spectroscopy on amorphous carbon films, J. Appl. Phys. 80 (1996) 440–447, https://doi.org/10.1063/1.362745.
[51] A. Sadezky, H. Muckenhuber, H. Grothe, R. Niessner, U. Pöschl, Raman microspectroscopy of soot and related carbonaceous materials: Spectral analysis and structural information, Carbon 43 (2005) 1731–1742, https://doi.org/10.1016/j.carbon.2005.02.018.